A Noise Model for a Charge-Coupled Device Pixel

R. Daniel McGrath, Polaroid Corporation, Cambridge, MA 02139
(617)577-5588, MCGRATD@mr.polaroid.COM

I. Introduction.

The noise in an imager can be viewed as a tree of noise contributors which add in quadrature. The total noise in a charge-coupled device branches into that which is present in the dark and that which is due to illumination. The dark contribution has a temporal branch related to the buffer and external circuitry, a temporal branch due to the shot noise of the dark signal, and a spatial fixed-pattern branch. The illuminated branch has a temporal branch due to the shot noise of the photocharge and a spatial branch which is dominated by geometric variations in the pixel aperture. The least understood of these contributions is the spatial fixed-pattern noise in the dark.

The understanding of noise in a charge-coupled device pixel begins with an understanding of noise in the dark. This must comprehend the dark current, which depends on the nature and location of interface and bulk generation sites. It must comprehend electric field enhancement, both due to enhanced generation and to impact ionization, because modern pixel design is a trade-off of increased charge handling capacity against high fields. It must comprehend geometric effects since process tolerances can become significant as the device size shrinks. Only then can the this be extended to illuminated pixels through the addition of photon statistics and geometric effects and to total noise through an understanding of buffer and signal chain noise[1].

A model has been developed for the spatial fixed-pattern and temporal noise in a pixel and will be compared with experimental results for a 6 µm by 12 µm pixel (Figure 1). It is concluded that in the dark that the noise is primarily due to statistical distributions of dark current generating defects, an effect that dominates over geometric variations. The model assumes (1) that the pixel can be subdivided into a series of depletion volumes each with a dominant defect, (2) that these defects generate dark current through the Shockley-Reed-Hall process[2], and (3) that these defects are few in number and their number varies randomly from pixel to pixel[3,4]. Field enhancement enters as an increase in generation rate, but does not play a significant role for typical operation. The noise is dominated by interface states in the channel and bulk defects in channel stop regions which received heavy implants[5]. While geometric effects dominate the spatial noise in the case of illumination, they are negligible in the dark case.

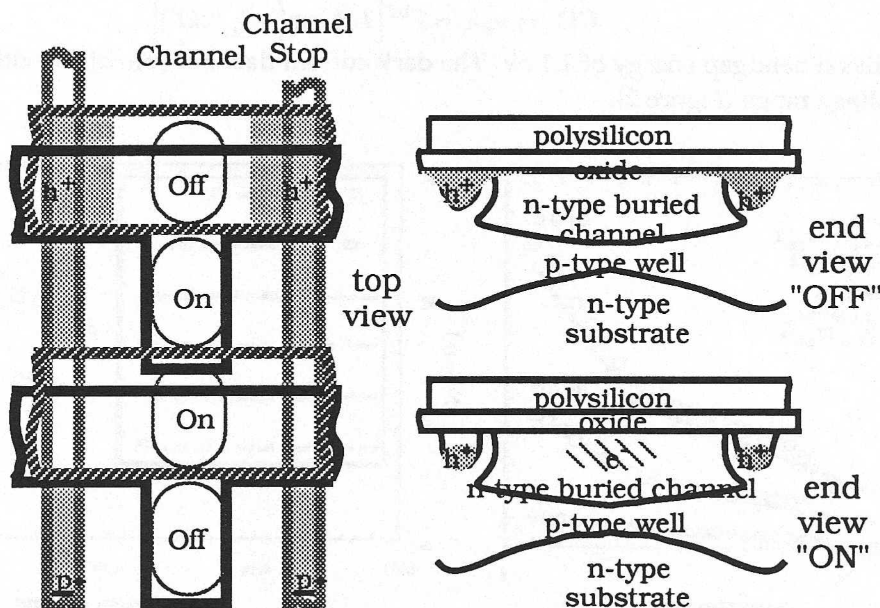

Figure 1: Pixel Layout (h^+ are free holes; e^- are free electrons)

II. Model

To allow direct comparison with experimental results the model account for the operation of an imager array which is operated with an integration time and a readout time. For a single defect type the temporal noise expressed in units of carriers is treated as a shot noise on the dark signal in the charge packet, including charge collected during image integration and readout and is given by

$$n_{temporal} = \sqrt{q_{dark}} = \sqrt{g\alpha_{pixel}d_{defects}\left(t_{\text{int}} + N_{row}t_{row}\right)}$$

where q_{dark} is the dark signal, g is the mean generation rate per defect, α_{pixel} is the pixel area, $d_{defects}$ is the defect density, t_{int} is the image integration time, t_{row} is the read time per row, and N_{row} is the row location in the image. As a result it is found to increase in subsequent lines in the imaging array due to dark current collected during readout. The spatial fixed-pattern noise is dominated by the charge generated during integration since the contribution that the charge packet picks up during readout is the ensemble contribution of all the pixels through which it passes during readout. It is given by

$$n_{spatial} = gt_{\text{int}}\sqrt{\alpha_{pixel}d_{defects}\left(1+\alpha_{pixel}d_{defects}\delta^2_{geometry}\right)\left(1+N_{row}\left(t_{row}/t_{\text{int}}\right)^2\right)}$$

where $\delta_{geometry}$ is the fractional variation of linear pixel dimension. It is directly proportional to the generation rate and only weakly dependent on the position in the image array. These results can be extended to multiple defects by adding the noise components in quadrature.

III. Theory Without Electric Field Enhancement.

The dominant process for generating dark current in silicon is charge generation mediated by single traps located in the bandgap[2,6]. The generation rate is

$$U = \sigma v_{th}N_t\left(pn - n_i^2\right)/\left(n + p + 2n_i\cosh\{(E_t - E_i)/kT\}\right)$$

where σ is the geometric mean of the electron and hole capture cross-sections, v_{th} is the carrier thermal velocity, N_t is the number of traps, n and p are the free carrier concentrations for electrons and holes, n_i is the intrinsic carrier concentration, E_t is the trap energy level, E_i is the intrinsic Fermi energy level, k is the Boltzmann constant and T is the absolute temperature. The generation rate has a strong dependence on E_t-E_i so that any traps with energies at mid-gap ($E_t = E_i$) will dominate. Assuming these to be the only important contributors, the temperature dependence is

$$U(T) \propto v_{th}n_i \propto T^{1/2}\left[T^{3/2}\exp(-E_g/2kT)\right]$$

where E_g is the silicon bandgap energy of 1.1 eV. The dark current data are consistent with this approximation over the whole voltage range (Figure 2).

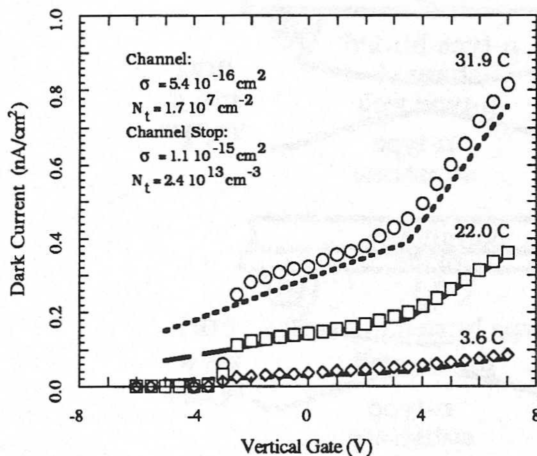

Figure 2

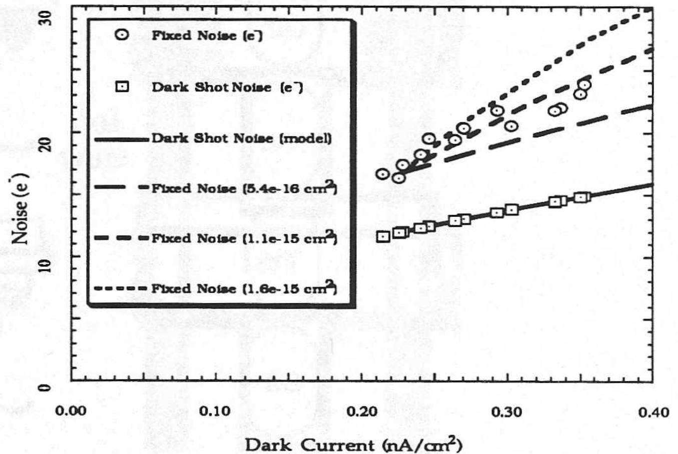

Figure 3

The maximum generation occurs when n and p are zero (i.e., when the material is fully depleted). The functional dependence of generation rate on free carrier concentration is $U(n,p)/U_{\max} \propto 2(np-n_i^2)/(n_i(n+p+2n_i))$. The definition of a depletion region for dark current generation is then $n,p \le 100 n_i$ which is a lower threshold than in the standard depletion approximation[7]. The voltage dependence of the dark current generating volumes can be estimated using a two-dimensional device model (e.g., TMA CANDE).

IV. Theory With Electric Field Enhancement.

Charge-coupled device design is often a tradeoff between performance and high electric fields, F. One mechanism through which these fields could increase dark current is the secondary ionization as photocharge passes through regions of high electric field. Electrons have a significantly higher ionization rate than holes so typically a fraction of the photoelectrons in transit will produce a single ionization event. The data for the electron ionization coefficient[8] is fit empirically by $I = a \cdot \exp\{-b/F\}$ with a = $1.38{\cdot}10^4$ cm^{-1} and b = $4.42{\cdot}10^5$ V/cm for $F <$ $2{\cdot}10^5$ V/cm and a = $7.34{\cdot}10^5$ cm^{-1} and b = $1.70{\cdot}10^6$ V/cm for $F > 2{\cdot}10^5$ V/cm

A second mechanism is through enhancing the generation rate for defects located in high field regions[9]. The electric field leads to a barrier lowering for a carrier collected in the trap which enhances the generation rate by a factor (1+Γ). $\Gamma \cong 2\sqrt{3\pi}(F/F_\Gamma)\left(1+(F/F_\Gamma)^2\right)$ for $F \ll F_\Gamma = \sqrt{24m^*(kT)^3}/q\hbar$ where m^* is the effective carrier mass, q the electron charge and $\hbar$ is Planck's constant. This introduces only a weak change in the temperature dependence so that this effect would appear as an increase in the generation rate due to increase in the apparent capture cross-section with increasing field.

V. Experiment

The model can be applied to a 72 μm^2 four-phase pixel with vertical anti-blooming (Figure 1). The active area where photogenerated and dark charge are collected is bounded laterally by the channel stops and vertically by the barrier in the p-well formed by the n-p-n doping structure. For nominal operation the gate alternates between an "off" voltage, -4V, and an "on" voltage, +6V. In the "off" condition the channel stops are accumulated and an inversion layer extends along the interface part way toward the center of the pixel. If the gate voltage is raised from -5V the edge of the inversion layer moves from the center of the channel back toward the channel stops leaving a larger area of the interface depleted. Above +3.5V the channel stops themselves deplete and a depletion volume connected to the active region increases in depth with increasing voltage. The photosites, which are without gates, remain depleted at the "off" voltage.

The imager is characterized using two modes. Operated as a gated diode, all the image array gates are set to a common voltage and the current through the reset diode is measured. Operated as an imager, the image array gates are cleared, two phases are held "on" for image integration, and then the array is read out. The spatial fixed-pattern noise is determined from the standard deviation of a small area in a mean frame; the temporal noise is determined by subtracting in quadrature the fixed-pattern noise and the noise from the on-chip buffer and external electronics. The dark current is the signal divided by the collection time and the pixel area. The four-phase pixel has two phases in the "off" state and two in the "on" state, so that the dark current is the combination of the two states, and the range of gate biases is limited to those for which the imager is functional.

VI. Results & Discussion

Measuring the dark current in the gated diode mode results in three linear segments (Figure 2). Below -3V the pixel dumps all of its charge to the substrate and background current from the test system is seen. Between -3V and +3.5V, the dark current increases linearly. Above +3.5V it increases linearly with a higher slope. This can be explained by treating the pixel for dark current purposes as two volumes: one consisting of the channel which is always active and the other consisting of the depleted volume of the channel stop which is only active for gate biases above +3.5V.

It is informative to sweep the "on" gate bias and plot the temporal noise and the fixed-pattern noise versus the dark current (Figure 3). The temporal noise is the shot noise on the dark charge and increases as a square root of dark signal independent of the capture cross-section and other details of the defect distribution.

The fixed-pattern noise depends on the capture cross-section. For a given dark current, a higher capture cross-section means a larger generation rate for each defect, fewer defects in each pixel and a larger variation in the number of defects from pixel to pixel resulting in a larger fixed-pattern noise. A lower capture cross-section on the other hand means a smaller generation rate per defect, more defects in each pixel and less variation from pixel to pixel.

For example, the pixel dark current of 200 pA/cm^2 at a gate voltage of 3.5V corresponds to the channel only being depleted. The temporal noise and fixed-pattern noise correspond to $\sigma = 5.4 \cdot 10^{-16}$ cm^2 and $N_t = 5.6$ defects/pixel or a defect density of $1.1 \cdot 10^7$ cm^{-2}. As the voltage is raised the channel stop begins to deplete and the defects there begin to contribute to the dark current. The larger the cross-section the more dramatic is the increase. The defects in the channel stop region are characterized by $\sigma = 1.1 \cdot 10^{-15}$ cm^2 (Figure 3). The dark current increase of 24.5 pA/cm$^2 \cdot$V corresponds to a defect density of $2.4 \cdot 10^{13}$ defects/cm^3 or $N_t = 3.6$ defects/pixel in the channel stop for the nominal biases.

The cross-section for the channel defects is close to the $6 \cdot 10^{-16}$ cm^2 quoted in the literature for interface states[7]. The higher cross-section for the channel stop is interpreted as bulk defects created by the high-dose implant process used to create this doping.

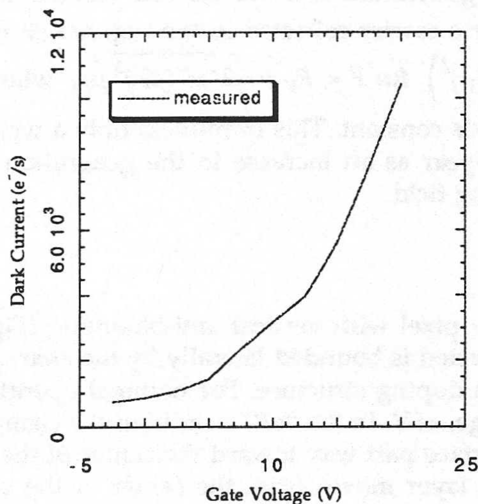

Figure 4

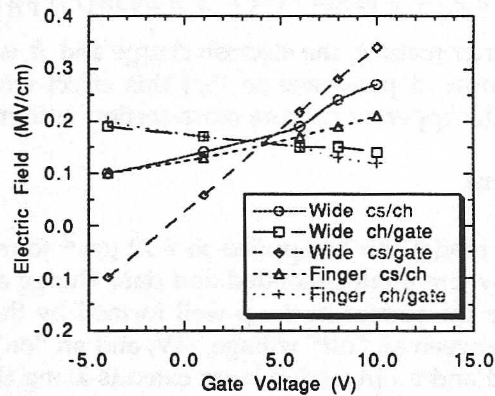

Figure 5

For gate voltages above 12 V there is a non-linear increase in the dark current (Figure 4). The device model can be used to determine the electric field between the channel stop and channel ("cs/ch") where ionization would occur and at the interface over the channel stop ("cs/gate") where enhanced generation is most likely (Figure 5). Predictions of the dark current are then generated for ionization only, for enhanced generation only and both combined (Figure 6). It is found that the enhanced generation increases too rapidly with gate voltage and that the effect is well fit by ionization alone.

VII. Conclusions

These resulting capture cross-sections and defect densities can be used as process parameters to predict device performance. The voltage dependence of the pixel design can be predicted in conjunction with a device simulation. The temperature dependence of the noise can also be predicted (Figure 7), but the strong temperature dependence requires accurate temperature measurements. In contrast to the random noise, the dependence of fixed-pattern noise on dark current is much different depending on whether the change is due to temperature, which is a change in generation rate and is linear, or is due to defect density (Figure 3). The fixed-pattern noise in an image array increases directly with integration time, but very weakly on readout time as the readout process averages the defect variation along a column.

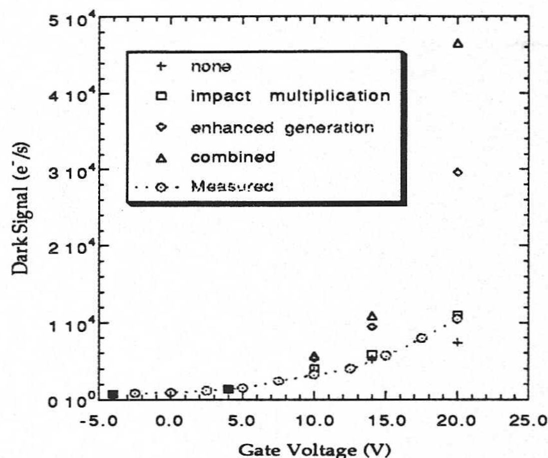

Figure 6

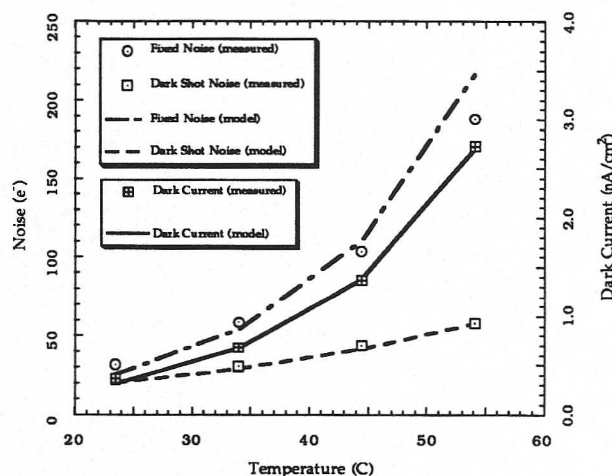

Figure 7

For the device dark current and noise can be explained by depletion volumes increasing with gate voltage and there is no significant field enhancement. This is true even though fields reach $3{\cdot}10^5$ V/cm. This analysis also provides direction for process development. For the pixel given here, the channel stop region was identified as providing excess dark current and noise and has been targeted for improvement. Finally this model predicts that as the density of the dominant defect decreases so that there are just a few per pixel, the fixed-pattern noise becomes more significant compared to the random noise. However, eliminating a defect entirely, as in the case of the bulk defect in the channel stop, significantly reduces the fixed-pattern noise and changes this balance.

VIII. Acknowledgments.

I appreciate the experimental support and encouragement I received for this work from Selim Bencuya, Peter Duane, Sufia Haque-Ahmed and Steve Clark of Polaroid. This work would not have been possible without the fine devices fabricated by the people of the Polaroid Microelectronics Laboratory.

VIII. References.

[1] P.Centen, IEEE Trans. Electron Devices, Vol ED-38, 1206-1216, 1991

[2] A.S.Grove, **Physics and Technology of Semiconductor Devices**, John Wiley and Sons, New York, 1967.

[3] R.D.McGrath et.al., IEEE Trans. Electron Devices, Vol ED-34, 2555-2557, 1987.

[4] W.McColgin et.al., IEDM 1992 Technical Digest, 113-116, 1992.

[5]R.D.McGrath et.al., Microelectronic Engineering, 19, 627-630, 1992.

[6] B.E.Burke and S.A.Gajar, IEEE Trans. Electron Devices, Vol ED-38, 285-290, 1991.

[7] E.H.Nicollian and J.R.Brews, **MOS (Metal Oxide Semiconductor) Physics and Technology**, John Wiley and Sons, New York, 1982.

[8] M.V.Fischetti, IEEE Trans. Electron Devices, Vol ED-38, 634-649 1991.

[9] G.A.M.Hurkx et.al., IEEE Trans. Electron Devices, Vol ED-39, 331-338, 1992.